Pergamon

Int. J. Solids Structures Vol. 35, No. 14, pp. 1617–1633, 1998

0020-7683/98 $19.00 + .00

PII: S0020-7683(97)00123-6

MIXED MODE FRACTURE IN EPICYCLOID SPECIMENS. I—THERMAL INCLUSIONS

H. GAO
Division of Applied Mechanics, Durand Building, Stanford University, Stanford, CA 94305, U.S.A.

W. H. MÜLLER and G. KEMMER
Laboratorium für Technische Mechanik, FB 10, Universität-Gesamthochschule-Paderborn, Pohlweg 47-49, 33098 Paderborn, Germany
E-mail: jmull1@ltm.uni-paderborn.de

(*Received* 3 *September* 1996; *in revised form* 20 *April* 1997)

Abstract—The technique of complex potentials is used to derive an analytical solution for the stresses that develop in epicycloidal specimens subjected to hot spot loading. The solution gives stress intensity factors for cusp-like cracks in such specimens which can be considered as a generalization of the traditional Griffith crack. It is shown that by suitable positioning of the hot spot the complete range of mode mixety, as well as negative mode I stress intensity factors, can be obtained. This illustrates the potential of epicycloid specimens for testing of bimaterial fracture properties as well as failure under compressive loading without frictional contact of crack surfaces. The paper concludes with a first experimental measurement of K_I in order to validate this new concept. © 1998 Elsevier Science Ltd.

1. INTRODUCTION

The successful use and application of advanced composite materials require testing and measurement of fracture properties, such as bond or adhesive strength, under essentially arbitrary mixed mode loading conditions. In the past it proved to be difficult to design mixed mode fracture specimens that reliably cover the complete range of mode mixety. An example of such an effort is the Brazil-nut-sandwich specimen, which is explained in detail in the paper by Wang and Suo (1990) or, in summary, in the monograph by Hutchinson and Suo (1991).

Moreover, experimental difficulties may arise when interpenetration or contact of the crack faces occur. In fact, this is an inherent feature of bimaterial interface fracture [cf Hutchinson and Suo (1991) p. 86]. Usually, the contact zone is tiny when compared to relevant physical features at the crack tip, such as a plastic zone. However, in a shear-dominated case the contact zones can become macroscopic and eventually will become an important issue (Rice, 1988).

In this paper the potential of epicycloid specimens for experimental determination of interface fracture properties will be investigated. By the very nature of an epicycloid such specimens a priori contain a defect in the form of a cusp which, as will be shown, can be considered as a generalization of the traditional Griffith-type of crack. The epicycloid specimens can be subjected to various types of thermo-mechanical loads. After a brief reminder on epicycloids (Section 2) a procedure will be developed to compute the stresses resulting from such loading (Section 3). Based on Muskhelishvili's formulation of two-dimensional elasticity an analytical solution for the complex potentials will be derived, which is then specialized to the case of a hot spot inclusion. Other loading types, such as dislocations or loading by point forces, will be discussed in a subsequent paper (Müller and Gao, 1997a/b).

Section 4 is devoted to the computation and discussion of stress intensity factors at epicycloidal cusps subjected to stresses which originate from a hot spot. In particular, a new interpretation and meaning of failure under negative mode I stress intensity, K_I, without

extensive contact of crack faces will be given. It is worth emphasizing that the solution for the stress intensity factors is in closed-form and valid for a specimen of finite size.

In order to demonstrate the relevance and potential of epicycloidal specimens for measurement of fracture mechanics properties the outcome of first experiments for fracture toughness evaluation will be reported in Section 5. The experiments were performed with epicycloid specimens made of Araldite B, and they were based on the phase-shift method recently developed by Ferber *et al.* (1996). A more detailed experimental evaluation is in progress (Linnenbrock *et al.*, 1997).

2. EPICYCLOIDS AND THEIR RELATION TO CRACK PROBLEMS

Consider the configuration depicted in Fig. 1. A circle, K, of radius ρ rolls on the outside or inside of the periphery of another circle, L, of radius $n\rho$ where n denotes an arbitrary positive real number. Furthermore, consider a tracing point P at a distance $\varepsilon\rho < \rho$ from the center of the first circle. The curves which are generated by P during the rolling process are known as cycloids. They can be obtained from the following generic equation in parametric form:

$$x = R\left[\cos\vartheta \mp \frac{\varepsilon}{n\pm 1}\cos((n\pm 1)\vartheta)\right] \quad y = R\left[\sin\vartheta - \frac{\varepsilon}{n\pm 1}\sin((n\pm 1)\vartheta)\right]$$

$$R = (n\pm 1)\rho \tag{1}$$

where the two different signs refer to circles that roll on or within another circle, respectively. Depending on whether the revolving circle is situated on the outside or inside of the other circle the resulting curves are also known as epicycloids or hypocycloids, respectively.

Special choices of the parameters n and ε lead to different types of cycloids. Various possibilities are discussed and depicted in the handbook by Bronstein and Semendjajew (1976), p. 88. In this paper the choice $\varepsilon = 1$ is of particular interest. In this case, the tracing point P is located on the periphery of the revolving circle. A remarkable feature of the resulting cycloids is the formation of cusps, i.e. sharp transition points where the cycloid

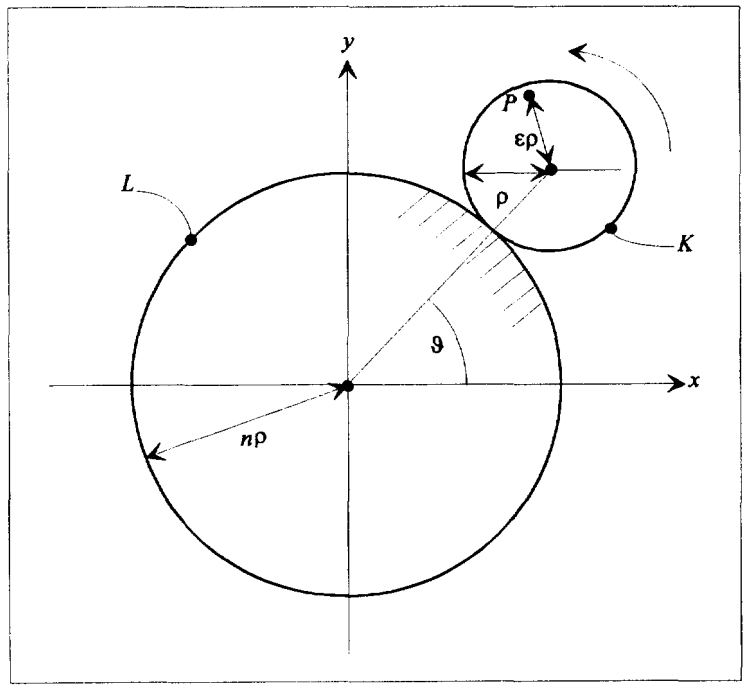

Fig. 1. On the generation of cycloids.

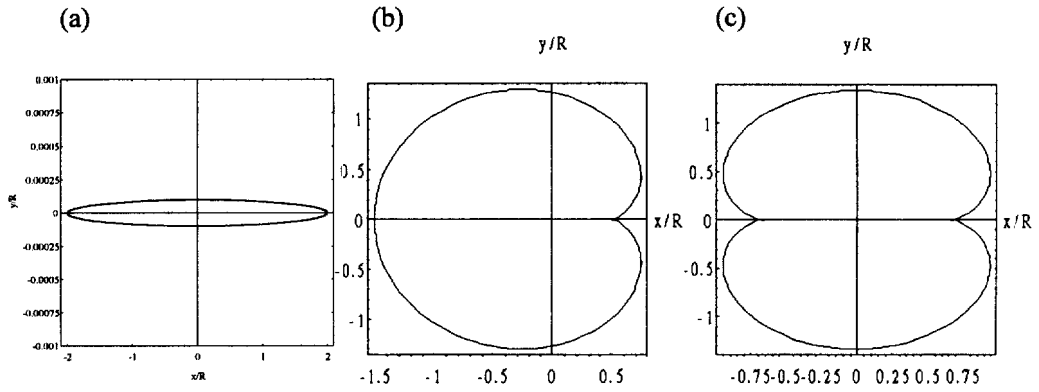

Fig. 2. Examples of cycloids with cusps: the Griffith crack (a); Pascal's limaçon (b); and the inverse Griffith crack (c).

reverses its direction of motion. Such cusps can be considered as a generalization of the pointed tips of Griffith cracks.

In fact the ordinary Griffith crack can be regarded as a special hypocycloid. Namely, if $\varepsilon = 1$ and if the stationary circle is twice as large as the revolving circle the generated curve degenerates into a straight line crack. This is illustrated in Fig. 2(a) for the choice $n = 2$, $\rho = 1$†. Figure 2(b, c) shows epicycloidal cusps, namely the cases $n = 1$, also known as Pascal's limaçon (Muskhelishvili, 1963), and $n = 2$, which corresponds an "inverse" Griffith crack.

In what follows, only closed cycloidal boundaries will be considered. Mathematically speaking this requires $n \in \mathbb{N}$, $\vartheta \in [0, 2\pi)$, $\varepsilon \in [0, 1]$. The area surrounded by such cycloids is subjected to thermo-mechanical loadings, in particular to a hot spot region, to dislocations, and to point forces. In the next section a comparatively general procedure will first be presented which allows us to compute the resulting stresses. The procedure is then specialized to the case of a hot spot. Other types of loading will be treated in subsequent papers. Moreover, the reaction of the crack tip or cusp singularity under thermo-mechanical loads, i.e. the case $\varepsilon = 1$, will be studied.

3. STRESS ANALYSIS THROUGH COMPLEX VARIABLE FORMULATION

3.1. *Basic relations*

Following the notation employed in the book by Sokolnikoff (1956) the complex stress potentials $\varphi(z)$ and $\psi(z)$ of the Muskhelishvili–Kolosov equations are introduced as follows

$$\begin{aligned} \sigma_{22} + \sigma_{11} &= 2[\varphi'(z) + \overline{\varphi'(z)}] \\ \sigma_{22} - \sigma_{11} + 2i\sigma_{12} &= 2[\bar{z}\varphi''(z) + \psi'(z)] \end{aligned} \tag{2}$$

where σ_{ij}, $i, j \in \{1, 2\}$ denote the stresses in Cartesian coordinates. Moreover, the resultant force, F, acting on a line, L, can be computed as follows:

$$F(z) = -\mathrm{i}[\varphi(\tilde{z}) + \tilde{z}\overline{\varphi'(\tilde{z})} + \overline{\psi(\tilde{z})}]_{\tilde{z}=a}^{\tilde{z}=z} \quad \forall z \in L \tag{3}$$

where $[]_{\tilde{z}=a}^{\tilde{z}=z}$ denotes the increase undergone by the expression in brackets as the point $\tilde{z}$ passes along the line L from points a to z.

3.2. *Determination of complex potentials for epicycloidal boundaries*

In the present case, the line, L, coincides with the periphery of an epicycloid which is supposed to be free of tractions. Hence, it is necessary and sufficient that the resulting force, F, vanishes in each and every point, z, of the periphery:

† For the purpose of illustration ε was chosen to be 1.0001 in this figure. In the case $\varepsilon \neq 1$ the curve is elliptical.

$$\varphi(z)+z\overline{\varphi'(z)}+\overline{\psi(z)}=0 \quad \forall z\in L. \tag{4}$$

The complex potentials are now separated into two parts. The first, characterized by the subscript "∞", denote the complex potentials of a hot spot in an infinite plane. The second, identified by the subscript "s", is chosen such that eqn (4) is satisfied:

$$\varphi(z)=\varphi_\infty(z)+\varphi_s(z) \quad \psi(z)=\psi_\infty(z)+\psi_s(z). \tag{5}$$

It follows that:

$$\varphi_s(z)+z\overline{\varphi_s'(z)}+\overline{\psi_s(z)}=-\varphi_\infty(z)-z\overline{\varphi_\infty'(z)}-\overline{\psi_\infty(z)} \quad \forall z\in L. \tag{6}$$

It is favorable to evaluate this equation in the plane of the unit circle. By application of the proper conformal mapping for epicycloids shown in eqn (1) which, alternatively, can be written as:

$$z=\omega(\zeta)=R\left(\zeta-\frac{\varepsilon}{n+1}\zeta^{n+1}\right) \quad \zeta=\exp(\mathrm{i}\vartheta) \quad \vartheta\in[0,2\pi) \tag{7}$$

it follows that

$$\varphi_s(\zeta)+\frac{\omega(\zeta)}{\overline{\omega'(\zeta)}}\overline{\varphi_s'(\zeta)}+\overline{\psi_s(\zeta)}=-\varphi_\infty(\zeta)-\frac{\omega(\zeta)}{\overline{\omega'(\zeta)}}\overline{\varphi_\infty'(\zeta)}-\overline{\psi_\infty(\zeta)} \quad \forall|\zeta|=1 \tag{8}$$

where

$$\frac{\omega(\zeta)}{\overline{\omega'(\zeta)}}=\zeta^{n+1}\frac{1-\dfrac{\varepsilon}{n+1}\zeta^n}{\zeta^n-\varepsilon} \qquad \bar{\zeta}=\zeta^{-1}. \tag{9}$$

The potentials φ_s and ψ_s are analytical within the unit circle and, consequently, can be represented by power series:

$$\varphi_s(\zeta)=\sum_{m=1}^{\infty}a_m\zeta^m \quad \psi_s=\sum_{m=1}^{\infty}b_m\zeta^m \tag{10}$$

where rigid body displacements have been ignored completely. If the Cauchy operator:

$$\frac{1}{2\pi\mathrm{i}}\oint_{|\zeta|=1}\frac{(\cdot)\,\mathrm{d}\zeta}{\zeta-\eta} \quad \forall|\eta|\leqslant 1 \tag{11}$$

is now applied to the first term on left-hand side of eqn (8) it follows that

$$\frac{1}{2\pi\mathrm{i}}\oint_{|\zeta|=1}\varphi_s(\zeta)\frac{\mathrm{d}\zeta}{\zeta-\eta}=\varphi_s(\eta)=\sum_{m=1}^{\infty}a_m\eta^m \quad \forall|\eta|\leqslant 1. \tag{12}$$

The second term in eqn (8) is divided into several parts which are analytical inside or outside of the unit circle, respectively:

$$\frac{1}{2\pi i}\oint_{|\zeta|=1}\left[\left(1-\frac{\varepsilon^2}{n+1}\right)\zeta-\frac{\varepsilon}{n+1}\zeta^{n+1}+\left(1-\frac{\varepsilon^2}{n+1}\right)\frac{\varepsilon\zeta}{\zeta^n-\varepsilon}\right]\overline{\varphi_s'}\left(\frac{1}{\zeta}\right)\frac{d\zeta}{\zeta-\eta}$$

$$=\frac{1}{2\pi i}\oint_{|\zeta|=1}\left[\left(1-\frac{\varepsilon^2}{n+1}\right)\zeta\sum_{m=1}^{\infty}m\overline{a_m}\zeta^{-m+1}\right]\frac{d\zeta}{\zeta-\eta}$$

$$+\frac{1}{2\pi i}\oint_{|\zeta|=1}\left[-\frac{\varepsilon}{n+1}\zeta^{n+1}\sum_{m=1}^{\infty}m\overline{a_m}\zeta^{-m+1}\right]\frac{d\zeta}{\zeta-\eta}$$

$$+\frac{1}{2\pi i}\oint_{|\zeta|=1}\left[\left(1-\frac{\varepsilon^2}{n+1}\right)\frac{\varepsilon\zeta}{\zeta^n-\varepsilon}\sum_{m=1}^{\infty}m\overline{a_m}\zeta^{-m+1}\right]\frac{d\zeta}{\zeta-\eta}\quad\forall|\eta|\leqslant 1. \tag{13}$$

Finally, integration of the third term of eqn (8) results in:

$$\frac{1}{2\pi i}\oint_{|\zeta|\to\infty}\bar{\psi}_s\left(\frac{1}{\zeta}\right)\frac{d\zeta}{\zeta-\eta}=\frac{1}{2\pi i}\oint_{|\zeta|\to\infty}\bar{\psi}_s\left(\frac{1}{\zeta}\right)\frac{d\zeta}{\zeta-\eta}=\frac{1}{2\pi i}\sum_{m=1}^{\infty}\oint_{|\zeta|=\infty}\bar{b}_m\frac{1}{\zeta^m}\frac{d\zeta}{\zeta-\eta}=0. \tag{14}$$

Consequently, it follows from eqn (6):

$$\sum_{m=1}^{\infty}(a_m\eta^m)+\left(1-\frac{\varepsilon^2}{n+1}\right)\overline{a_1}\eta-\frac{\varepsilon}{n+1}\sum_{m=1}^{n+1}(m\overline{a_m}\eta^{n-m+2})$$

$$=\frac{1}{2\pi i}\oint_{|\zeta|=1}\left[-\varphi_\infty(\zeta)-\frac{\omega(\zeta)}{\overline{\omega'(\zeta)}}\overline{\varphi'_\infty(\zeta)}-\overline{\psi_\infty(\zeta)}\right]\frac{d\zeta}{\zeta-\eta}\quad\forall|\eta|\leqslant 1. \tag{15}$$

Constant terms have been ignored. From this equation the coefficients a_i, $i=1,\ldots,\infty$ can be identified which determines the complex potential φ_s. Equation (8) can then be used to obtain the second complex potential ψ_s.

3.3. *Stress intensity factors of epicycloidal cusps*

The characteristic shape of epicycloids will locally intensify stresses and strains. As it was mentioned before the choice $\varepsilon=1$ leads to cusp-like cracks. Due to symmetry it is sufficient to consider the cusp located on the positive x-axis at a distance a (which corresponds to the location $\zeta=1$) and to study the behavior of its SIFs as a function of all possible positions z_0 of the center of the hot spot. The stress intensity factors (SIFs), K_I and K_{II}, for that cusp can be determined from the following asymptotic form for the complex potential [see, e.g. Kanninen and Popelar (1985)]:

$$K_I-iK_{II}=-\lim_{z_c\to 0}\{2\sqrt{-2\pi z_c}\varphi'(z_c)\} \tag{16}$$

where the distance from the crack tip, z_c, can be identified in Fig. 3. Moreover, by a Taylor series expansion of the conformal mapping shown in eqn (7) it follows that:

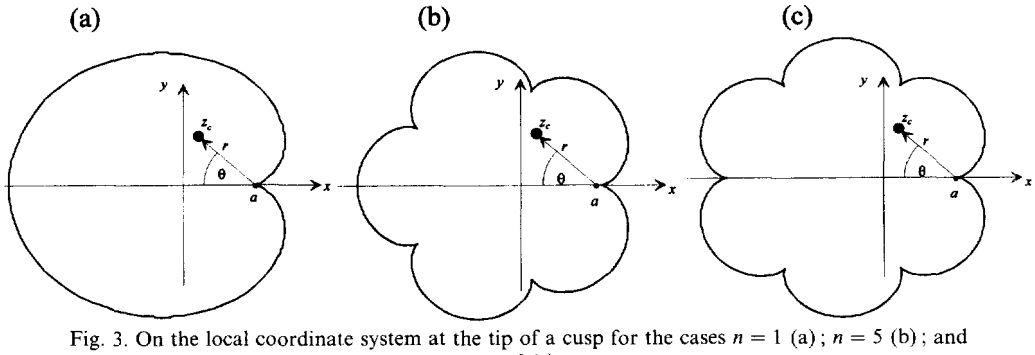

Fig. 3. On the local coordinate system at the tip of a cusp for the cases $n=1$ (a); $n=5$ (b); and $n=6$ (c).

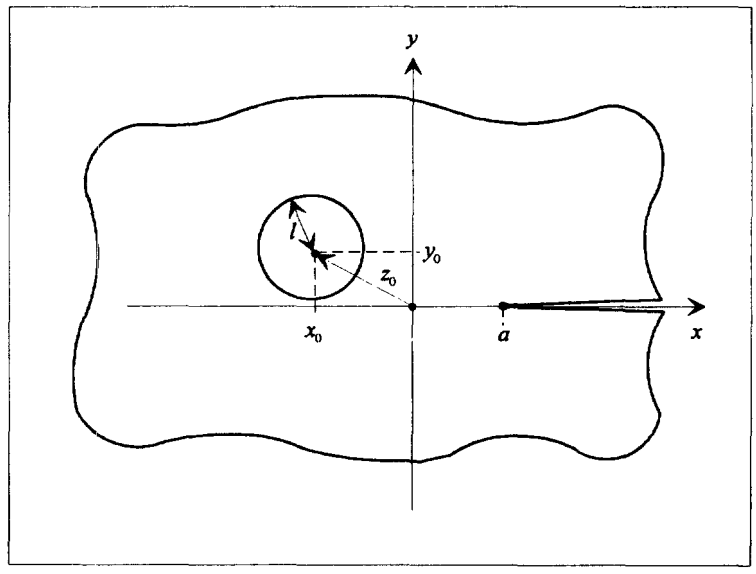

Fig. 4. On the geometry of a semi-infinite crack in an infinite plate in front of a hot spot.

$$z_c = z - a = -\frac{Rn}{2}(\zeta - 1)^2 \tag{17}$$

and since

$$\varphi'(z) = \frac{d\zeta}{dz}\varphi'(\zeta) \tag{18}$$

eqn (16) can be evaluated and yields

$$K_I - iK_{II} = 2\sqrt{\frac{\pi}{(n+1)a}}\varphi'(\zeta = 1) \qquad a = \frac{n}{n+1}R. \tag{19}$$

3.4. *The special case of a hot spot in an epicycloid*

The complex potentials for a circular hot spot of radius l and strength c at a position z_0 of an infinite plane (see also Fig. 4) are given by (Muskhelishvili, 1963):

$$\varphi_\infty = \begin{cases} -\dfrac{c(z-z_0)}{2l^2} & \forall |z-z_0| < l \\ 0 & |z-z_0| > l \end{cases} \qquad \psi_\infty = \begin{cases} 0 & \forall |z-z_0| < l \\ -\dfrac{c}{z-z_0} & \forall |z-z_0| > l \end{cases} \tag{20}$$

with:

$$c = \frac{4\mu}{1+\kappa}\varepsilon^{th}l^2, \quad \varepsilon^{th} = \Delta\alpha\,\Delta T, \quad \kappa = \begin{cases} 3-4\nu, & \text{plane strain} \\ \dfrac{3-\nu}{1+\nu}, & \text{plane stress} \end{cases} \tag{21}$$

where μ is the shear modulus, ν is Poisson's ratio, $\Delta\alpha$ refers to the difference in thermal expansion coefficients of the regions in and around the thermal spot, and ΔT is the change in temperature with respect to the stress-free configuration. In this solution differences in the elastic constants of the hot spot region and the surrounding epicycloidal matrix have been ignored.†

† See Section 5 for a discussion of the influence of elastic mismatch.

This will now be inserted into the right-hand side (RHS) of eqn (15) to yield:

$$\text{RHS} = \frac{1}{2\pi i}\oint_{|\zeta|=1}[-\overline{\psi_\infty(\zeta)}]\frac{d\zeta}{\zeta-\eta} = \frac{1}{2\pi i}\oint_{|\zeta|=1}\left[\frac{c}{\overline{\omega(\zeta)}-\overline{\omega(\zeta_0)}}\right]\frac{d\zeta}{\zeta-\eta}$$

$$= \frac{1}{2\pi i}\oint_{|\zeta|=1}\left[\frac{-c\zeta}{(\zeta-\bar{\zeta}_0^{-1})\bar{f}(\zeta^{-1})\bar{\zeta}_0}\right]\frac{d\zeta}{\zeta-\eta} \quad \forall|\eta| \leqslant 1 \tag{22}$$

where:

$$f(\zeta) = R\left(1-\frac{\varepsilon}{n+1}\frac{\zeta^{n+1}-\zeta_0^{n+1}}{\zeta-\zeta_0}\right) \tag{23}$$

provided the hot spot region is not situated on the epicycloidal boundary. The remaining integral can be evaluated to obtain:

$$\text{RHS} = \frac{c}{\bar{\zeta}_0(1-\eta\bar{\zeta}_0)\overline{f(\zeta_0)}} - \frac{c}{\bar{\zeta}_0\overline{f(0)}}$$

$$= \frac{c}{R\bar{\zeta}_0}\left(\frac{1}{(1-\varepsilon\bar{\zeta}_0^n)(1-\eta\bar{\zeta}_0)}-1\right) = \frac{c}{R(1-\varepsilon\bar{\zeta}_0^n)}\frac{\eta}{1-\eta\bar{\zeta}_0}+\cdots \tag{24}$$

where constants have been omitted in the last step. This result is now expanded into a power series and inserted into eqn (15):

$$\sum_{m=1}^{\infty}(a_m\eta^m)+\left(1-\frac{\varepsilon^2}{n+1}\right)\overline{a_1}\eta-\frac{\varepsilon}{n+1}\sum_{m=1}^{n+1}(m\bar{a}_m\eta^{n-m+2}) = \bar{c}^*\sum_{m=0}^{\infty}(\bar{\zeta}_0^m\eta^{m+1}) \tag{25}$$

where

$$c^* = \frac{c}{R(1-\varepsilon\zeta_0^n)}. \tag{26}$$

A comparison of corresponding powers of both sides yields:

$$\eta^1: a_1+\left(1-\frac{\varepsilon^2}{n+1}\right)\overline{a_1}-\varepsilon\bar{a}_{n+1} = \bar{c}^*$$

$$\eta^i: a_i-\frac{\varepsilon}{n+1}(n+2-i)\bar{a}_{n+2-i} = \bar{c}^*\bar{\zeta}_0^{i-1} \quad i=2,\ldots,n+1$$

$$\eta^j: a_j = \bar{c}^*\bar{\zeta}_0^{j-1} \quad j>n+1. \tag{27}$$

The elimination of $\bar{a}_{n+1}$ in $(27)_1$ by means of the last equation of $(27)_2$ leads to:

$$\text{Re}(a_1) = \frac{1}{2}\frac{n+1}{n+1-\varepsilon^2}(\bar{c}^*+\varepsilon c^*\zeta_0^n) \tag{28}$$

which allows one to determine a_{n+1}

$$a_{n+1} = \bar{c}^* \bar{\zeta}_0^n + \frac{\varepsilon}{n+1}[\mathrm{Re}(a_1) - \mathrm{i}\,\mathrm{Im}(a_1)]. \tag{29}$$

The imaginary part of a_1 corresponds to a rigid body rotation since:

$$\varphi_s(\zeta) = [\mathrm{Re}(a_1) + \mathrm{i}\,\mathrm{Im}(a_1)]\zeta + a_2\zeta^2 + \ldots + \left(\bar{c}^* \bar{\zeta}_0^n + \frac{\varepsilon}{n+1}[\mathrm{Re}(a_1) - \mathrm{i}\,\mathrm{Im}(a_1)]\right)\zeta^{n+1} + \ldots \tag{30}$$

and, therefore,

$$\mathrm{i}\,\mathrm{Im}(a_1)\left(\zeta - \frac{\varepsilon}{n+1}\zeta^{n+1}\right) = \mathrm{i}\,\mathrm{Im}(a_1)\frac{z}{R}. \tag{31}$$

In what follows it will be neglected. The rearrangement of the remaining equations in $(27)_2$ yields:

$$a_{2+k} = \frac{(n+1)^2}{(n+1)^2 - \varepsilon^2(n-k)(2+k)}\left[\bar{c}^* \bar{\zeta}_0^{1+k} + \frac{\varepsilon}{n+1}(n-k)c^* \zeta_0^{n-k-1}\right]$$

$$a_{n-k} = \bar{c}^* \bar{\zeta}_0^{n-k-1} + \frac{\varepsilon}{n+1}(2+k)\bar{a}_{2+k} \tag{32}$$

where

$$k = \begin{cases} 0, \ldots, (n-3)/2, & \text{if } n \text{ odd} \\ 0, \ldots, (n-4)/2, & \text{if } n \text{ even} \end{cases}. \tag{33}$$

In the second case the set of equations shown in eqn (32) needs to be supplemented by:

$$a_{n/2+1} - \frac{\varepsilon}{n+1}\left(\frac{n+2}{2}\right)\bar{a}_{n/2+1} = \bar{c}^* \bar{\zeta}_0^{n/2} \tag{34}$$

or more explicitly

$$\mathrm{Re}(a_{n/2+1}) = \frac{2(n+1)}{2(n+1) - \varepsilon(n+2)}\mathrm{Re}(\bar{c}^* \bar{\zeta}_0^{n/2})$$

$$\mathrm{Im}(a_{n/2+1}) = \frac{2(n+1)}{2(n+1) + \varepsilon(n+2)}\mathrm{Im}(\bar{c}^* \bar{\zeta}_0^{n/2}). \tag{35}$$

The coefficients of eqn $(27)_3$ lead to a power series, which can be summed up as follows:

$$\sum_{m=n+2}^{\infty}(a_m \zeta^m) = \frac{\bar{c}^* \zeta^{n+1} \bar{\zeta}_0^n}{1 - \bar{\zeta}_0 \zeta} - \bar{c}^* \zeta^{n+1} \bar{\zeta}_0^n. \tag{36}$$

Consequently, the complex potential φ outside of the hot spot region can be written as:

$$\varphi(\zeta) = a_1\left(\zeta + \frac{\varepsilon}{n+1}\zeta^{n+1}\right)$$

$$+ \sum_{k=0}^{\delta_0}\left[a_{2+k}\zeta^{2+k} + \left(\frac{\varepsilon}{n+1}(2+k)\bar{a}_{2+k} + \bar{c}^*\bar{\zeta}_0^{n-k-1}\right)\zeta^{n-k}\right] + \frac{\bar{c}^*\zeta^{n+1}\bar{\zeta}_0^n}{1-\bar{\zeta}_0\zeta} + \delta_1 a_{n/2+1}\zeta^{(n+2)/2} \quad (37)$$

where

$$\delta_0 = \begin{cases}(n-3)/2, & \text{if } n \text{ odd}\\ (n-4)/2, & \text{if } n \text{ even}\end{cases} \qquad \delta_1 = \begin{cases}0, & \text{if } n \text{ odd}\\ 1, & \text{if } n \text{ even}\end{cases} \quad (38)$$

and constants a_1, a_{2+k}, $a_{n/2+1}$ are given by eqns (28), $(32)_1$ and (35), or more explicitly by:

$$a_1 = \frac{1}{2}\frac{n+1}{n+1-\varepsilon^2}\frac{1-\varepsilon^2(\zeta_0\bar{\zeta}_0)^n}{(1-\varepsilon\bar{\zeta}_0^n)(1-\varepsilon\zeta_0^n)}\frac{c}{R}$$

$$a_{2+k} = \frac{(n+1)^2}{(n+1)^2-\varepsilon^2(n-k)(2+k)}\left[\frac{\bar{\zeta}_0^{1+k}}{1-\varepsilon\bar{\zeta}_0^n} + \frac{\varepsilon(n-k)}{n+1}\frac{\zeta_0^{n-k-1}}{1-\varepsilon\zeta_0^n}\right]\frac{c}{R}$$

where

$$k = \begin{cases}0,\ldots,(n-3)/2, & \text{if } n \text{ odd}\\ 0,\ldots,(n-4)/2, & \text{if } n \text{ even}\end{cases} \quad (39)$$

and

$$\mathrm{Re}(a_{n/2+1}) = \frac{n+1}{2(n+1)-\varepsilon(n+2)}\left(\frac{\zeta_0^{n/2}}{1-\varepsilon\zeta_0^n} + \frac{\bar{\zeta}_0^{n/2}}{1-\varepsilon\bar{\zeta}_0^n}\right)\frac{c}{R}$$

$$\mathrm{Im}(a_{n/2+1}) = \mathrm{i}\frac{n+1}{2(n+1)+\varepsilon(n+2)}\left(\frac{\zeta_0^{n/2}}{1-\varepsilon\zeta_0^n} - \frac{\bar{\zeta}_0^{n/2}}{1-\varepsilon\bar{\zeta}_0^n}\right)\frac{c}{R} \quad n = 2,4,6,\ldots.$$

This representation explicitly shows the dependence of all relevant constants on the number of cusps, n, the sharpness of the cusp, ε, the position of the center of the hot spot, ζ_0, its strength, c [given in eqn $(21)_1$], and on the size of the generating circles $R = (n+1)\rho$. Note that the upper limit δ_0 in eqn (38) is required to be positive for any given choice of n. Also recall that the second potential $\psi(z)$ follows from continuation by means of eqn (4):

$$\psi(\zeta) = -\overline{\varphi(\zeta)} - \frac{\overline{\omega(\zeta)}}{\omega'(\zeta)}\varphi'(\zeta). \quad (40)$$

In particular, for a hot spot located in the center (i.e. $\zeta_0 = 0$) the stress potentials assume the following simple form:

$$\varphi(\zeta) = \frac{c}{2R}\frac{n+1}{n+1-\varepsilon^2}\left(\zeta + \frac{\varepsilon}{n+1}\zeta^{n+1}\right), \quad \psi(\zeta) = -\frac{c}{R\zeta}\frac{1}{1-\varepsilon\zeta^n}. \quad (41)$$

The SIFs for a cusp at position $z = a$ follow from eqn (19) in combination with the expression for the stress potential (37):

$$K_{\mathrm{I}}-\mathrm{i}K_{\mathrm{II}}=2\sqrt{\frac{\pi}{(n+1)a}}\left\{2a_1+\sum_{k=0}^{\delta_0}\left[(2+k)a_{2+k}+\left(\frac{2+k}{n+1}\bar{a}_{2+k}+\bar{c}^{*}\bar{\zeta}_0^{n-k-1}\right)(n-k)\right]\right.$$
$$\left.+\frac{\bar{c}^{*}\bar{\zeta}_0^{n}[n(1-\bar{\zeta}_0)+1]}{(1-\bar{\zeta}_0)^2}+\delta_1\frac{n+2}{2}a_{n/2+1}\right\} \quad (42)$$

which for a hot spot in the center reduces to:

$$K_{\mathrm{I}}=2c\sqrt{\frac{\pi}{(n+1)a^3}}\quad K_{\mathrm{II}}=0. \quad (43)$$

The constants a_1, a_{2+k}, $a_{n/2+1}$ can directly be read off from eqns (39) if the sharpness parameter, ε, is set equal to one. For normalization of this expression the stress intensity factors, $K^{\infty}_{\mathrm{I/II}}$, of a semi-infinite crack in front of a hot spot (see Fig. 4) are very useful:

$$K_{\mathrm{I}}^{\infty}-\mathrm{i}K_{\mathrm{II}}^{\infty}=c\sqrt{\frac{\pi}{2}}\frac{\exp\left(\mathrm{i}\frac{3}{2}\arctan\frac{y_0}{a-x_0}\right)}{[(a-z_0)(a-\bar{z}_0)]^{3/4}} \quad (44)$$

as will be outlined in the following section. For a derivation of this result compare Müller *et al.* (1996).

4. DISCUSSION OF THE RESULTS

4.1. *Pascal's limaçon*

For the case $n = 1$ or, in other words, for Pascal's limaçon the general solution for the SIFs shown in eqn (42) reduces to:

$$\frac{K_{\mathrm{I}}-\mathrm{i}K_{\mathrm{II}}}{|K_{\mathrm{I}}^{\infty}-\mathrm{i}K_{\mathrm{II}}^{\infty}|}=\left|1-\frac{z_0}{a}\right|^{3/2}\left[2\frac{1-\bar{\zeta}_0\zeta_0}{(1-\zeta_0)(1-\bar{\zeta}_0)}+2\frac{\bar{\zeta}_0}{(1-\bar{\zeta}_0)^2}+\frac{\bar{\zeta}_0^2}{(1-\bar{\zeta}_0)^3}\right]. \quad (45)$$

Note that the singularity of $\varphi'(\zeta = 1)$ at the cusp, i.e. at position $\zeta_0 = 1$, is eliminated by the normalization factor since:

$$z_0=2a\zeta_0(1-\tfrac{1}{2}\zeta_0). \quad (46)$$

Figure 5 presents the mode I and II SIFs separately for every possible position of the hot

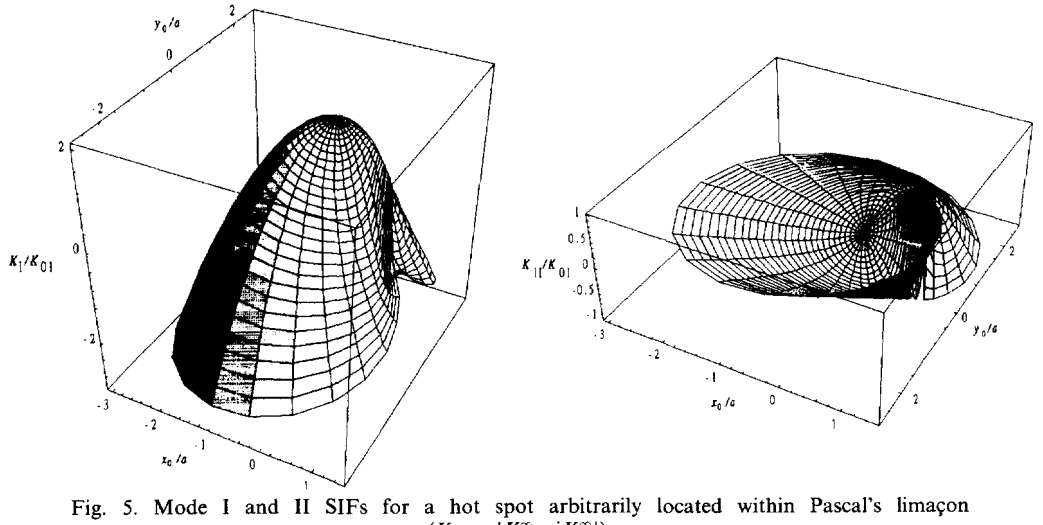

Fig. 5. Mode I and II SIFs for a hot spot arbitrarily located within Pascal's limaçon ($K_{01} = |K_{\mathrm{I}}^{\infty}-\mathrm{i}K_{\mathrm{II}}^{\infty}|$).

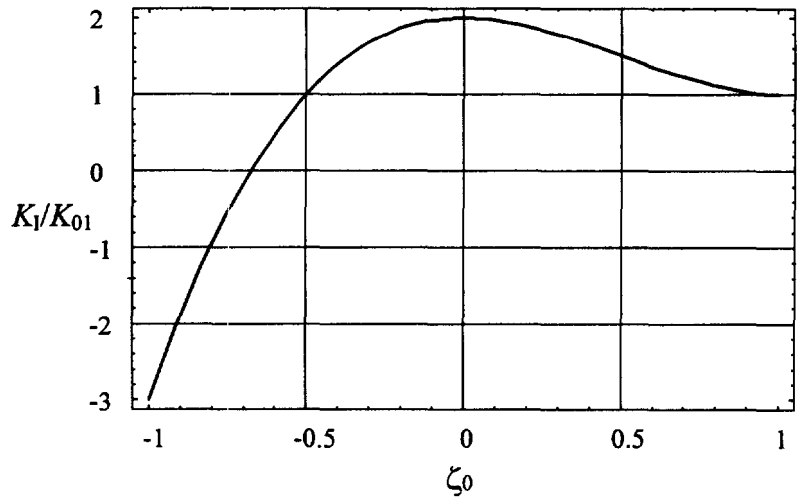

Fig. 6. Mode I SIFs for a hot spot located along the line of symmetry of Pascal's limaçon ($K_{01} = |K_I^\infty|$).

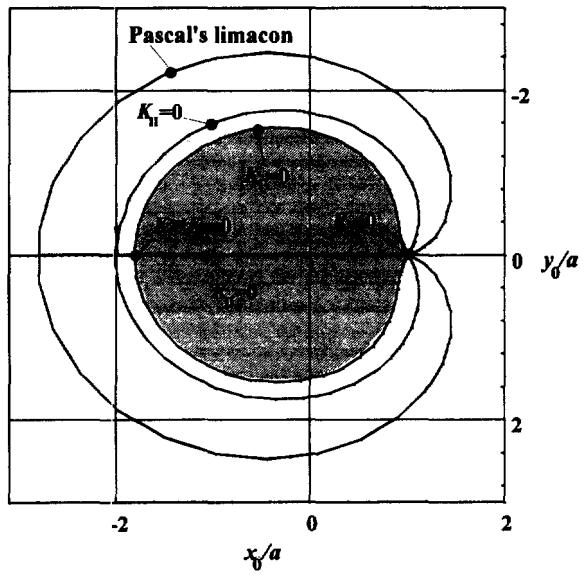

Fig. 7. Line of blind spots for Pascal's limaçon ($K_I = 0$ or $K_{II} = 0$); the shaded area corresponds to positive K_I-values.

spot within the epicycloid. The purpose of this figure is a qualitative illustration of the overall behavior of the SIFs. Quantitative data should be obtained directly from eqn (45) or, for the symmetrical loading case, from Fig. 6. Note that geometrical quantities, such as the radius, l, of the hot spot or radius of the epicycloid, ρ, are implicitly taken into account through the normalization factor $K_{01} = |K_I^\infty - iK_{II}^\infty|$, i.e. by means of eqns $(19)_2$, (21) and (44). Furthermore note that along its axis of symmetry K_{II}† must vanish and the cusp is subjected to mode I loading only.‡ Figures 6 and 7 allow us to study this aspect in more detail. For convenience the region of positive K_I-values is shaded. Finally, Fig. 8 shows the absolute value of mixed mode SIFs $|K_I - iK_{II}|$, together with the phase angle or "mixety":

$$\Psi = \arctan\frac{K_{II}}{K_I}. \tag{47}$$

The following features are worth mentioning:

† where K_{II}^∞ also vanishes

‡ The "overlapping effect" in Fig. 5 around the tip of the cusp is an artefact attributed to the use of the drawing routines of Mathematica® which represent the steep gradients imperfectly.

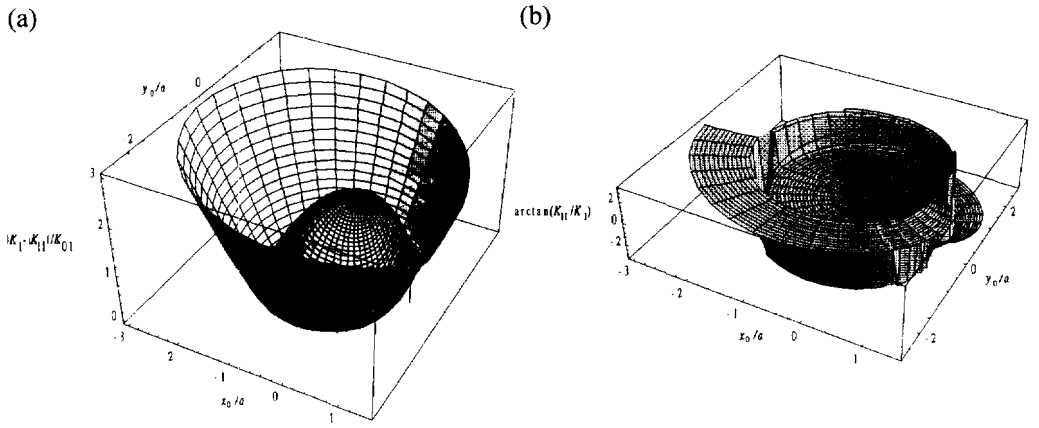

Fig. 8. Absolute value of mixed mode SIFs (a); and angle of mixety (b).

- As shown in Fig. 7 there exist curves of blind spots where either the mode I or the mode II SIF vanish. In particular there is a blind spot where $K_I = K_{II} = 0$, i.e. where loading of the cusp changes from compression to tension for vanishing shear.
- As indicated qualitatively in Fig. 5 and shown quantitatively in Fig. 6 the region of negative mode I in combination with a vanishing or a non-vanishing mode II contribution is comparatively large and also very intense. This clearly illustrates the potential epicycloid specimens for investigation of compressive fracture. If the center of an "expanding" hot spot is first located at a position close to the crack tip, then, intuitively speaking, the flanks of the cusp are separated, which corresponds to positive K_I-values. Now, if the center of this hot spot is moved along the real axis through the origin and on to the border of Pascal's limaçon, which is opposite to the cusp, then the flanks are finally bent toward each other and this corresponds to negative K_Is.
- As shown qualitatively in Fig. 8(b) the complete range of mixety, i.e. $-90° \leqslant \Psi \leqslant 90°$ can be covered by suitable positioning of a hot spot within the epicycloid. This behavior is depicted quantitatively in Fig. 9 for a special choice of hot spot centers, namely those which are located along the line $\zeta_0 = ir$, $r \in [0, 1)$. It should be emphasized that this was done merely for illustration purposes and that the mode mixety for any positioning can easily be computed from the analytical eqn (45).
- As shown in Fig. 6 the K_I-factor of a finite-sized cusp can be intensified by a factor of two when compared to the mode I SIF of a semi-infinite crack. This must be attributed to a focusing effect of the finite geometry of Pascal's limçon.

4.2. *The inverse Griffith crack*

For an epicycloid where $n = 2$, i.e. for an inverse Griffith crack, the general solution for the SIFs shown in eqn (42) reduces to:

$$\frac{K_I - iK_{II}}{K_{02}} = \frac{4}{3}\left|1 - \frac{z_0}{a}\right|^{3/2}\left|1 + \frac{z_0}{a}\right|^{3/2}\left\{\frac{3}{2}\left(\frac{1}{1-\bar{\zeta}_0^2} + \frac{\zeta_0^2}{1-\zeta_0^2}\right)\right.$$
$$\left. + \frac{\bar{\zeta}_0^2[2(1-\bar{\zeta}_0)+1]}{(1-\bar{\zeta}_0^2)(1-\bar{\zeta}_0)^2} + \left[6\,\mathrm{Re}\left(\frac{\bar{\zeta}_0}{1-\bar{\zeta}_0^2}\right) + i\frac{6}{5}\,\mathrm{Im}\left(\frac{\bar{\zeta}_0}{1-\bar{\zeta}_0^2}\right)\right]\right\} \quad (48)$$

where

$$K_{02} = \frac{c}{a^{3/2}}\sqrt{\frac{\pi}{3}}\left|\frac{a}{a-z_0}\right|^{3/2}\left|\frac{a}{a+z_0}\right|^{3/2}. \quad (49)$$

This normalization guarantees that all data in the subsequent SIF plots remain finite even if the hot spot is moved toward the two cusps at $z_0 = \pm a$.

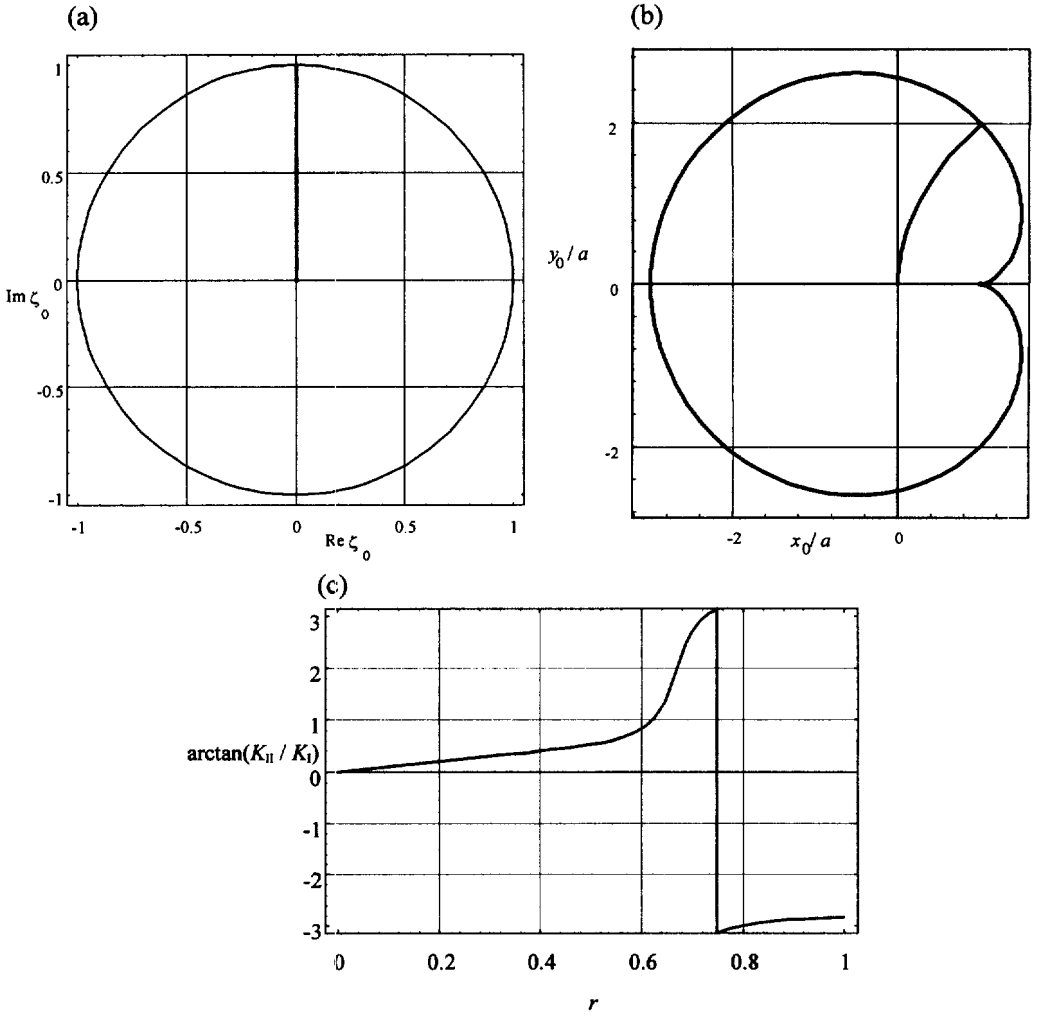

Fig. 9. Location of centers of blind spots along $\zeta_0 = ir$, $r \in [0, 1)$ (plane of the unit circle (a); mapping plane (b); and corresponding angle of mixety (c).

Figures 10–13 present various views of the SIFs for an epicycloid of degree $n = 2$. They are analogous to the SIFs shown in Figs 5–8 for Pascal's limaçon. All previous remarks hold accordingly.

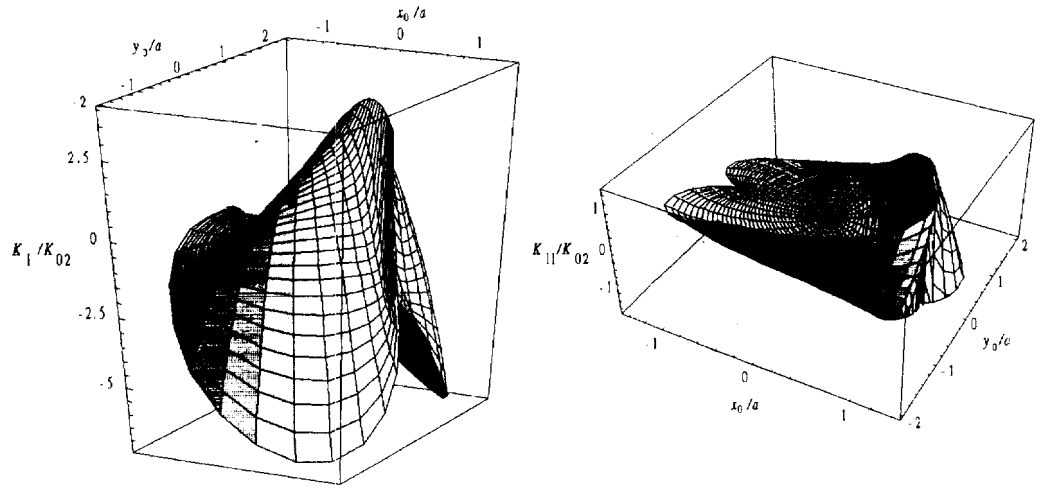

Fig. 10. Mode I and II SIFs for a hot spot arbitrarily located within an epicycloid of degree $n = 2$.

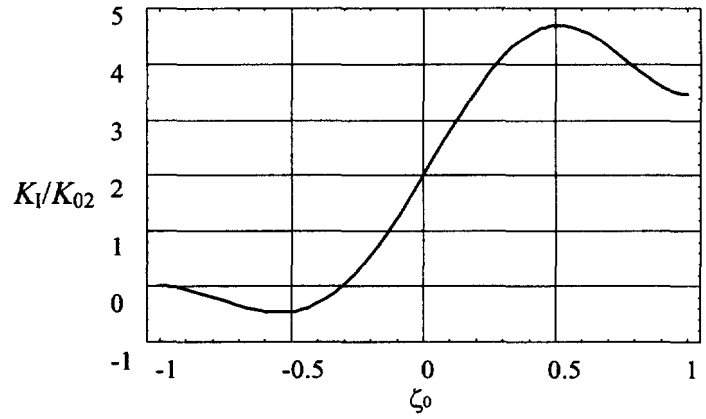

Fig. 11. Mode I SIFs for a hot spot located along the line of symmetry of an epicycloid of degree $n = 2$.

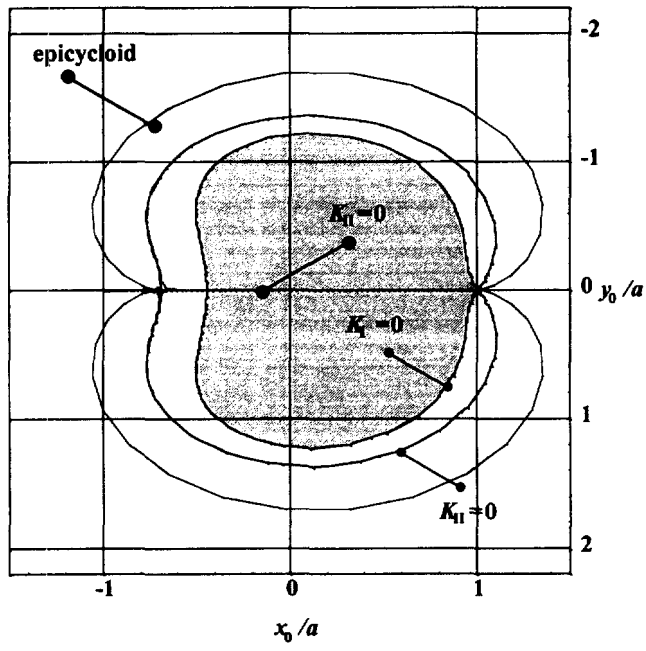

Fig. 12. Line of blind spots for an epicycloid of degree $n = 2$; the region of positive K_I-values is shaded.

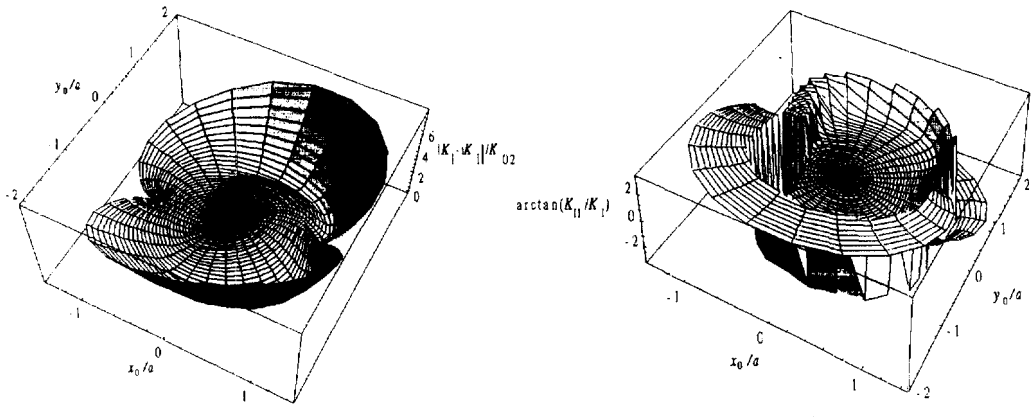

Fig. 13. Absolute value of mixed mode SIFs and angle of mixety for an epicycloid of degree $n = 2$.

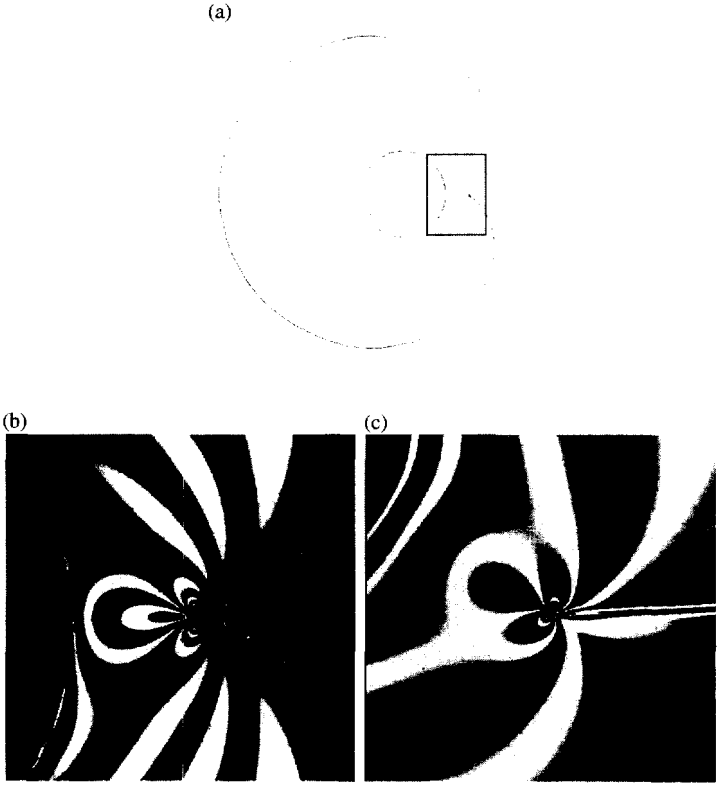

Fig. 14. Araldite B specimen of an epicycloid of degree $n = 1$ with a hot spot region made of Porcelin and isochromatic fringe patterns in the vicinity of a cusp-like crack ($a = 30$ mm, $2l = 43$ mm, $\zeta_0 = 0$, $\Delta K = -48$ K; by courtesy of Linnenbrock and Ferber, Laboratorium für Technische Mechanik) juxtaposed to the fringe patterns of a Griffith crack slightly sidewards of a hot spot region.

5. FIRST EXPERIMENTAL VALIDATION

An epicycloid specimen (Pascal's limaçon) made of Araldite B with a hot spot region made of porcelin was inserted into a polariscope. Figure 14(a) shows the specimen together with the photoelastic fringe pattern, Fig. 14(b), observed during the experiment. In order to demonstrate visually that cusps are part of a "family" of crack-like objects the (mixed-mode) fringe pattern around the tip of a Griffith crack in a rectangular plate (140×140 mm^2, crack length 35 mm) slightly sidewards of a hot spot region was added in Fig. 14(c).† The similarity of the near tip stress fields is apparent.

After cooling the isochromatic fringe patterns shown in Fig. 14(b) were used to determine experimentally the stress intensity at the cusp. The analysis was based on the procedures described in Ferber *et al.* (1996). Essentially, use was made of the basic equation of photoelasticity:

$$\left(\frac{\sigma_{rr}(r_i, \varphi_i) - \sigma_{\varphi\varphi}(r_i, \varphi_i)}{2}\right)^2 + \tau_{r\varphi}^2(r_i, \varphi_i) - \left(\frac{Sn_i}{2B}\right)^2 = 0 \tag{50}$$

in combination with Williams' solution for the near tip stress field of straight cracks including the higher-order terms (Williams, 1957). Here, S denotes the photoelastic constant, n_i is the order of an isochromatic fringe, B is the thickness of the specimen, and (r_i, φ_i) refer to the polar coordinates of a point of measurement, i.e. to a pixel i of the digitized fringe as measured from the crack tip. The SIFs $K_{I/II}$ as well as the coefficients a_2, a_3, a_4, b_3 and b_4 of Williams' solution are the unknowns to be determined from the resulting system of nonlinear equations.

† The reader interested in the experimental evaluation of mode II SIFs is referred to the paper by Ferber *et al.* (1996) and to the other references cited therein.

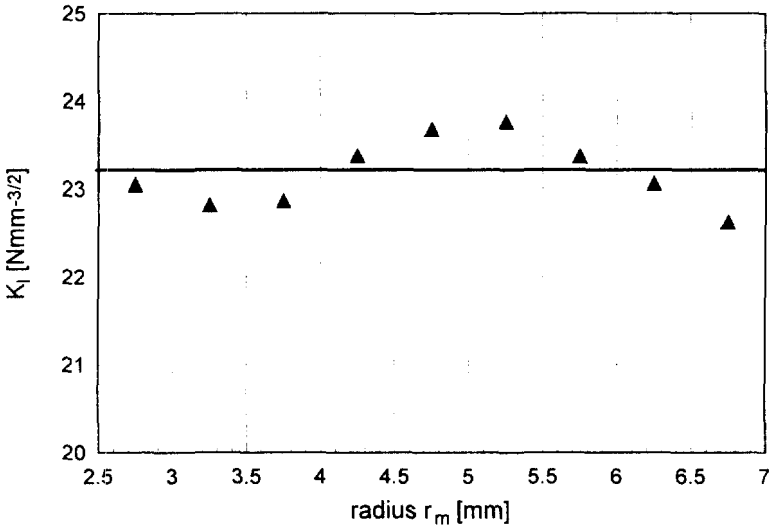

Fig. 15. SIF K_I for an epicycloid made of Araldite B (by courtesy of Linnenbrock and Ferber, Laboratorium für Technische Mechanik).

Figure 15 shows the experimental results for the mode I SIF which was evaluated over regions of different size around the crack tip. The size of the region is indicated by the radius r_m. The following table contains a few materials data relevant to the experiment:

	Poisson's ratio	Young's modulus/ N/mm^2	Thermal expansion coefficient 10^{-6} 1/K
Araldite B	0.374	3300	41
Porcelin	0.28	199,000	8

The arithmetic average of the SIF is shown as a line in Fig. 15 and given by:

$$K_I = 23.2\ \mathrm{N/mm^{3/2}}. \tag{51}$$

This agrees surprisingly well with the predicted value for K_I which can easily be obtained from equation (43) with $c = 2809$ N, $n = 1$, $a = 30$ mm:†

$$K_I = 21.4\ = \mathrm{N/mm^{3/2}}. \tag{52}$$

To account for the elastic mismatch the following first-order correction [see Müller *et al.* (1996)] was used:

$$K_I = \frac{1+\alpha}{1+\alpha-2\beta} 2c \sqrt{\frac{\pi}{(n+1)a^3}} = 26.6\,\mathrm{N/mm^{3/2}} \tag{53}$$

where α and β denote Dundurs' parameters. This equation seems to overestimate the stress intensity.

6. CONCLUSIONS AND OUTLOOK

The intent of this paper was to draw attention to the potential of epicycloid specimens in fracture mechanics testing. To this end an analytical solution for the stresses in such specimens wâs derived, based on complex potential theory, and specialized to the case of

† For this result the elastic coefficients of Araldite B (see table) were used.

hot spot loading: eqns (37)–(40). The solution was used to derive closed-form expressions for the mixed mode stress intensity factors of the cusp-like cracks existing in these specimens: eqns (42) and (43). This solution was further specialized to specific epicycloids, namely to Pascal's limaçon as well as to the so-called inverse Griffith crack. It was demonstrated that by suitable positioning of the hot spot it is possible to establish any desired degree of mode mixety. Moreover, if the hot spot is located in certain blind spot areas pure mode I or mode II loading conditions can be arranged. Finally, it is also possible to obtain negative pure mode I conditions without contact and shear of crack flanks (Figs 7 and 12). It is worth emphasizing that the closed-form equations for the SIFs can also be used for testing of interface properties, such as toughness of a welded or glued zone. For example, a Pascal's limaçon specimen can be separated along its line of symmetry and reattached, similarly to other sandwich-type of specimens, such as symmetric double cantilever beams (Cao and Evans, 1989) or the Brazil-nut specimen (Hutchinson and Suo, 1991; Wang and Suo, 1990).

Moreover, photoelasticity was used to experimentally determine the mode I stress intensity factor for an epicycloidal cusp. The analysis based on Williams' solution for straight cracks lead to SIF which agreed fairly well with the theoretically predicted value. However, further experiments, in particular for mixed mode loading, seem necessary to establish the usefulness of epicycloid specimens for testing of bimaterial as well as compressive fracture. Furthermore, Williams' solution needs to be reconsidered and eventually be extended to the concept of cusps and, finally, other types of loading conditions should be examined. All this is left to future research.

Acknowledgements—The foundation to this paper was laid during a sabbatical visit of one of the authors (H.G.) to the Universität-Gesamthochschule-Paderborn at the beginning of 1996. The stay was financially supported by the Kommission für Forschung und wissenschaftlichen Nachwuchs der Universität Paderborn. This support is gratefully acknowledged. The authors would also like to thank the head of the Laboratorium für Technische Mechanik, o. Professor Dr rer. nat. K. P. Herrmann, for his hospitality and support. Special thanks are due to the lab members, Dipl.-Ing. K. Linnenbrock and Dr.-Ing. F. Ferber for their engagement in the experiments presented in the paper.

REFERENCES

Bronstein, I. N. and Semendjajew, K. A. (1976) *Taschenbuch der Mathematik*, 16. Auflage. Verlag Harri Deutsch, Zürich.

Cao, H. C. and Evans, A. G. (1989) An experimental study of the fracture resistance of bimaterial interfaces. *Mechanics of Materials* **7**, 295–304.

Ferber, F., Herrmann, K. P. and Linnenbrock, K. (1996) Elementary failure analysis of composite models by using optical methods of stress analysis and modern digital image systems. In *Engineering Systems Design and Analysis*. Vol. 4. ASME, New York, PD-Vol. 76.

Hutchinson, J. W. and Suo, Z. (1991) Mixed mode cracking in layered materials. In *Advances in Applied Mechanics*. Vol. 29, eds J. W. Hutchinson and T. Y. Wu. Academic Press, New York.

Kanninen, M. F. and Popelar, C. H. (1985) *Advanced Fracture Mechanics*. Oxford University Press, New York and Clarendon Press, Oxford.

Linnenbrock, K., Ferber, F., Gao, H. and Müller, W. H. (1997) Mixed mode fracture in epicycloid specimens IV: experimental validation (in preparation).

Müller, W. H. and Gao, H. (1997a) Mixed mode fracture in epicycloid specimens II. Point force loading. *International Journal of Solids & Structures* **35**, 205–217.

Müller, W. H. and Gao, H. (1997b) Mixed mode fracture in epicycloid specimens III. Dislocations. *International Journal of Solids & Structures* (submitted).

Müller, W. H., Gao, H., Chiu, C.-H. and Schmauder, S. (1996) A semi-infinite crack in front of a circular, thermally mismatched heterogeneity. *International Journal of Solids and Structures* **33**(5), 731–746.

Muskhelishvili, N. I. (1963) *Some Basic Problems of the Mathematical Theory of Elasticity*, 4th edn. Noordhoff, Groningen, The Netherlands.

Rice, J. R. (1988) Elastic fracture mechanics concepts for interfacial cracks. *Journal of Applied Mechanics* **55**, 98–103.

Sokolnikoff, I. S. (1956) *Mathematical Theory of Elasticity*, 2nd edn. McGraw-Hill, New York.

Wang, J.-S. and Suo, Z. (1990) Experimental determination of interfacial toughness curves using Brazil-nut-sandwiches. *Acta Metallica Materiala* **38**(7), 1279–1290.

Williams, M. L. (1957) On the stress distribution at the base of a stationary crack. *Journal of Applied Mechanics* **24**, 109–114.